Predictions of Optic Nerve Traction Forces and Peripapillary Tissue Stresses Following Horizontal Eye Movements

Xiaofei Wang,[1] Liam K. Fisher,[1] Dan Milea,[2,3] Jost B. Jonas,[4,5] and Michaël J. A. Girard[1,2]

[1]Ophthalmic Engineering and Innovation Laboratory, Department of Biomedical Engineering, Faculty of Engineering, National University of Singapore, Singapore
[2]Singapore Eye Research Institute, Singapore National Eye Center, Singapore
[3]Duke-NUS, Singapore
[4]Department of Ophthalmology, Medical Faculty Mannheim of the Ruprecht-Karls-University, Heidelberg, Germany
[5]Beijing Institute of Ophthalmology, Beijing Tongren Eye Center, Beijing Tongren Hospital, Capital Medical University, and Beijing Key Laboratory of Ophthalmology and Visual Sciences, Beijing, China

Correspondence: Michaël J.A. Girard, Ophthalmic Engineering and Innovation Laboratory, Department of Biomedical Engineering, National University of Singapore, Engineering Block 4, #04-8, 4 Engineering Drive 3, 117583 Singapore; mgirard@nus.edu.sg.

Submitted: December 18, 2016
Accepted: March 14, 2017

Citation: Wang X, Fisher LK, Milea D, Jonas JB, Girard MJA. Predictions of optic nerve traction forces and peripapillary tissue stresses following horizontal eye movements. *Invest Ophthalmol Vis Sci*. 2017;58:2044–2053. DOI:10.1167/iovs.16-21319

Purpose. To use finite element (FE) analysis to predict the optic nerve sheath traction forces that act on the optic nerve head (ONH) following horizontal eye movements, and the resulting stress levels in the peripapillary connective tissues of the ONH (Bruch's membrane [BM] and sclera).

Methods. An FE model of a healthy eye was reconstructed in primary gaze position that included details from the orbital and ONH tissues. Optic nerve sheath traction forces and peripapillary tissue stresses in both adduction and abduction (13°) were computed using FE analysis.

Results. Our models predicted that, following eye movements, the ONH was sheared in the transverse plane due to the pulling action of the optic nerve. The optic nerve sheath traction forces were 90 mN in abduction and 150 mN in adduction. Peripapillary tissue stresses were concentrated in the nasal and temporal quadrants. In adduction, scleral stresses were highest in the temporal region, and BM stresses were slightly higher in the nasal region. This trend was reversed in abduction.

Conclusions. Following eye movements, our models predicted high optic nerve sheath traction forces of the same order of magnitude as extraocular muscle forces. Optic nerve traction resulted in significant peripapillary stresses, and thus may have a role to play in the development of peripapillary zones, glaucoma, and myopia.

Keywords: eye movements, peripapillary zones, Bruch's membrane, sclera, finite element analysis, glaucoma, myopia

The peripapillary region of the optic nerve head (ONH) shows several distinct zones that have been categorized into a peripheral alpha zone (presence of Bruch's membrane [BM] with irregular RPE), a beta zone (absence of RPE and presence of BM), and a central gamma zone (absence of BM).[1] We know that the beta zone is correlated with glaucoma[2–5] and high myopia.[1,6] Additionally, the zones also can occur in healthy individuals without any pathologic conditions.[3,7,8] However, the exact mechanism for the development and progression of the peripapillary zones has so far remained unclear. Previous studies[9,10] have shown that the development of the beta zone might be associated with elevated IOP, possibly resulting from the sliding of the RPE on BM as induced by IOP.[9] Jonas et al.[11,12] postulated that the gamma zone is associated with axial elongation in high myopic eyes. These studies suggest a mechanical role in the genesis of peripapillary zones.

In the early 19th century, eye movements had been suggested to be able to deform the optic nerve and cause functional changes of the eye. A detailed review of this literature is given by Sibony.[13] Recently, there has been renewed interest in the effects of eye movements on the optic nerve and ONH deformations and their possible links to optic neuropathies. Specifically, studies that used optical coherence tomography (OCT),[13–15] finite element (FE) modeling,[16] and magnetic resonance imaging (MRI),[17] all converge to the single fact that horizontal eye movements considerably deform the ONH tissues (through the "strong" optic nerve [including its sheath] traction imposed on the ONH), and that these deformations can be as large (or significantly larger) than those induced by a substantial IOP elevation.[14,16] Because eye movements appear to have a strong impact on the ONH tissues, and can even alter the axial length of the eye,[18] we aimed to understand if there could exist a link between eye movements and the development of peripapillary zones. To do so, an improved knowledge of the traction force of the optic nerve sheath following eye movements and its influence on the biomechanical environment of peripapillary tissues is required.

The aim of this study was to use FE modeling to estimate the magnitude of the optic nerve sheath traction force during horizontal eye movements, and estimate eye movement–

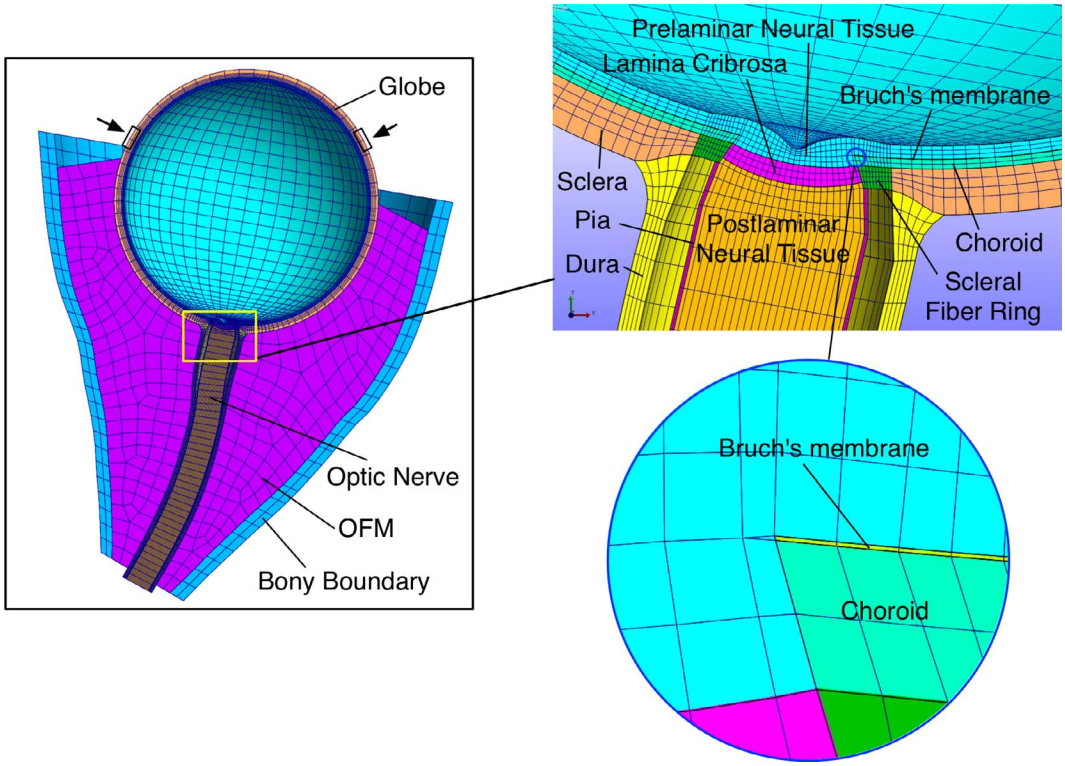

Figure 1. Reconstructed geometry and FE mesh of the eye movement model. Detailed ONH structures were included (sclera, LC, neural tissue, pia, dura, choroid, and BM) using average measurements from the literature. *Right bottom*: A zoomed image of the ONH region showing BM and choroid. *Arrows*: Muscle insertion regions. OFM, orbital fat-muscle complex.

induced stresses (internal forces) in peripapillary tissues (BM and sclera) where the peripapillary zones typically develop. To the best of our knowledge, such estimates have not yet been reported.

Methods

In this study, we used FE modeling to estimate the magnitude of the optic nerve sheath traction force, and peripapillary sclera (ppS) and peripapillary BM (ppBM) stresses following horizontal eye movements. FE analysis can provide a quantitative characterization of loaded structures, given information about three-dimensional geometry, material properties, and boundary/loading conditions. Because of the complexities exhibited by biological tissues, simplifying assumptions are usually necessary to achieve a solvable model. What we provide in this article is mostly an exploratory study of the potential effects of eye movements on the stress levels within peripapillary tissues. However, how these stresses/strains could contribute to the development of peripapillary zones or even glaucoma is currently unknown. We used FE to examine this new idea, which may help us identify potentially important parameters and provide directions for future experimental and clinical studies. Below is a detailed description of our FE simulations.

Geometry of the FE Model

The geometry of the FE model was modified from our previous study.[16] Briefly, the optic nerve, orbital fat, and eye globe were reconstructed from MRI images of a healthy subject. The ONH geometry, including the peripapillary sclera, scleral flange, prelaminar neural tissue, lamina cribrosa, postlaminar neural tissue, pia, and dura, was embedded within an "idealized" spherical corneoscleral shell. Detailed geometric parameters of these tissues can be found in the recent literature.[16] We further included the choroid and BM into the model to increase its biofidelity and to estimate stresses in the regions in which peripapillary zones typically develop. The thickness of the choroid and BM were 134 μm[19] and 5 μm,[20] respectively. Only half of the eye was reconstructed because the FE model was assumed symmetric about a transverse plane passing through the center of the eye globe (Fig. 1).

The reconstructed model was discretised into a hexahedron-dominant mesh with 36,836 eight-node hexahedra and 1512 six-node pentahedra elements using ICEM CFD (ANSYS, Inc., Canonsburg, PA, USA; Fig. 1). The mesh density was numerically validated through a convergence test.

Material Stiffness of the Reconstructed Eye Tissues

To simulate the biomechanical environment of the ONH during eye movements, a material stiffness (or more accurately, a set of biomechanical properties) needs to be assigned to each tissue. Biomechanical properties are essential parameters, as they provide a link between stress (force) and strain (deformation). To date, obtaining patient-specific biomechanical properties of eye tissues is not yet feasible. Therefore, we used averaged data reported in the literature as described below.

Both the sclera and lamina cribrosa (LC) were modeled as fiber-reinforced composites,[21] as in our previous model.[16] A scleral fiber ring with thickness of 0.5 mm was included (Fig. 1) to account for the circumferential alignment of collagen fibers within the scleral flange and around the scleral canal.[22] Collagen fibers in other scleral regions were organized randomly. The collagen fibers in the LC were more isotropic

TABLE. Tissue Biomechanical Properties Used for the Baseline Model

Tissue	Constitutive Model	Biomechanical Properties	References
Sclera	Mooney-Rivlin Von Mises distributed fibers	c1 = 0.805 MPa c3 = 0.0127 MPa c4 = 1102.25 kf = 2 (scleral ring) kf = 0 (other region of sclera) θp: preferred fiber orientations*	Girard et al.[56]
BM	Isotropic elastic	Elastic modulus = 10.79 MPa Poisson's ratio = 0.49	Chan et al.[58]
Choroid	Isotropic elastic	Elastic modulus = 0.6 MPa Poisson's ratio = 0.49	Friberg et al.[59]
Dura	Yeoh model	c1 = 0.1707 MPa c2 = 4.2109 MPa c3 = -4.9742 MPa	Wang et al.[16]
LC	Mooney-Rivlin Von Mises distributed fibers	c1 = 0.05 MPa c3 = 0.0025 MPa c4 = 100 kf = 1 θp: preferred fiber orientation†	Zhang et al.[22]
Neural tissue	Isotropic elastic	Elastic modulus = 0.03 MPa Poisson's ratio = 0.49	Miller[60]
Pia	Yeoh model	c1 = 0.1707 MPa c2 = 4.2109 MPa c3 = -4.9742 MPa	Wang et al.[16]
OFM	Isotropic elastic	Shear modulus = 900 Pa Poisson's ratio = 0.49	Schoemaker et al.[24]

* Collagen fibers in the scleral fiber ring were aligned circumferentially around scleral canal; fibers in other parts of the sclera were organized randomly.

† Collagen fibers in the LC were organized along the radial direction (from the central vessel trunk to the scleral canal).

than in the sclera, but organized along the radial direction (from the central vessel trunk to the scleral canal).[22] The neural tissue, orbital fat, choroid, and BM were modeled as isotropic linear materials and were thus described with a single stiffness value (elastic modulus). The pia and dura were simulated as isotropic nonlinear hyperelastic materials, with biomechanical properties derived from porcine tissues.[16] The orbital wall was modeled as a rigid body. The constitutive stress/strain relationships and biomechanical properties used for the baseline FE model are listed in the Table.

Friction Between Tissues, Boundary, and Loading Conditions

We assumed a frictionless contact between the posterior scleral surface and the orbital fat to account for the presence of Tenon's capsule.[23] The outer surface of the dura sheath was tied to the orbital fat based on our own MRI observation during eye movements (Wang X, Girard MJA, unpublished data, 2016), and that of others,[24] in which the surrounding fat tissues were found to be displaced together with the optic nerve. The contact between the pia and the dura was assumed frictionless, as both tissues are separated by the cerebrospinal fluid of the arachnoid space. The orbital fat was able to slide over the bony margin of the orbit with friction. All other tissues were bonded together by sharing nodes at the respective tissue boundaries. As the optic nerve is firmly held in position in the optic canal region,[25,26] the optic nerve was fixed at the orbital apex. The outer surface of the orbital wall was also fixed.

An IOP of 15 mm Hg (applied to the inner limiting membrane),[27] a cerebrospinal fluid pressure (CSFP) of 12.9 mm Hg (applied within the arachnoid space),[28] and an orbital tissue pressure of 4.4 mm Hg[29] (applied to the outer surface of globe and optic nerve) were used as initial loading conditions in the FE model. These values represent averaged normal pressures in the supine position.

A rotation of 13° (in both adduction and abduction) about the superoinferior axis through the center of the eye was directly applied at the lateral rectus muscles' insertion regions of the globe (as nodal displacements; Fig. 1).

Varying the Stiffness of Eye Tissues: FE Sensitivity Studies

The stiffness of eye tissues can vary considerably, even among healthy individuals.[30] This is likely to influence peripapillary tissue stresses and thus the potential development of peripapillary zones. Accordingly, we aimed to further investigate the sensitivity of ppBM stresses to variations in connective tissue stiffness. To this end, we used a design of experiments (DOE) approach[31] to investigate how variations in the stiffness of the sclera, dura, pia, and LC could influence stress levels in the ppBM. In the DOE analysis, a four-factor two-level full factorial analysis was used to allow examination of the effects of possible interactions between factors. A high and a low level were assigned to each factor. To rank the impact of factors, a reasonable physiological range of these factors should be used. Unfortunately, tissue stiffness data are scarce in the literature and, even when reported, the values can vary considerably across studies. Therefore, the low and high levels were set by varying the stiffness values by 20% around their baseline values to obtain their trends of effects (see Supplementary Material SA). A total of 16 FE simulations (see Supplementary Material SB), reflecting all possible combinations of high and low levels for each factor, were performed. The DOE results were postprocessed using MATLAB (Version 2015a; Mathworks, Inc., Natick, MA, USA).

FE Processing to Predict Optic Nerve Sheath Traction Force and Peripapillary Tissue Stresses

All models were solved using FEBio (Musculoskeletal Research Laboratories, University of Utah, Salt Lake City, UT, USA) in both adduction and abduction and for all aforementioned scenarios.[32] For the baseline eye movement models, we reported the traction force acting on the peripapillary sclera generated by the pulling action of the optic nerve dura sheath. Traction forces were reported along the deformed optic nerve direction defined from the ONH center to the orbital apex. Specifically, for each dura element adjacent to the sclera, the normal stress along the designated direction was derived from the stress tensor of the element; then this normal stress was multiplied by the area of the middle cross-section of the element to obtain the force value. The forces of all these elements were summed and reported as the traction force. This procedure was verified through another model in which the applied force was known. In the verification model, we found that the calculated traction force was in agreement with the prescribed force (within 5%).

Additionally, for each model, we reported the effective stress in the ppS and ppBM. Effective stress is an engineering measure that represents the local averaged internal forces experienced by tissues. The peripapillary tissues were divided into four sectors (nasal, temporal, superior, and inferior) and the mean effective stresses in each sector were reported. Because we constructed a half model with assumed symmetry, the superior and inferior sectors are essentially the same sector. In the sensitivity study, the mean effective stresses in all sectors of ppBM were reported.

Results

Predictions of the Traction Forces Generated by Optic Nerve Sheath Pulling

We evaluated the traction force generated by the optic nerve dura sheath along the deformed optic nerve direction (from the ONH center to the orbital apex as illustrated by the black arrows in Fig. 2). In the baseline model, the traction forces were 90 and 150 mN for abduction and adduction of 13°, respectively.

Peripapillary Tissue Deformations

During eye movements, peripapillary tissues were sheared in the transverse plane by the optic nerve sheath, which resulted in significant deformations within these tissues. Specifically, in adduction, we observed posterior displacements of temporal peripapillary tissues and anterior displacement of nasal peripapillary tissues (Fig. 2). In abduction, the deformation trend was reversed (Fig. 2).

Stress Predictions in Peripapillary Tissues

We reported effective stresses (mean value in each sector) for 13° adduction and abduction (Fig. 3). We found that, in general, the stresses experienced by the ppS and ppBM following either 13° adduction or abduction were significant. Specifically, the average stresses of ppS and ppBM following adduction were 0.19 and 0.25 MPa, respectively; those following abduction were 0.17 and 0.24 MPa, respectively.

In adduction, stresses in the temporal ppS (0.25 MPa) were higher than those in the nasal ppS (0.13 MPa), whereas stresses in the temporal ppBM (0.26 MPa) were lower than those in the nasal ppBM (0.27 MPa). In abduction, the stress distribution trend was reversed (Fig. 3). Specifically, the stresses in the temporal ppS, nasal ppS, temporal ppBM, and nasal ppBM were 0.12, 0.20, 0.26, and 0.24 MPa, respectively.

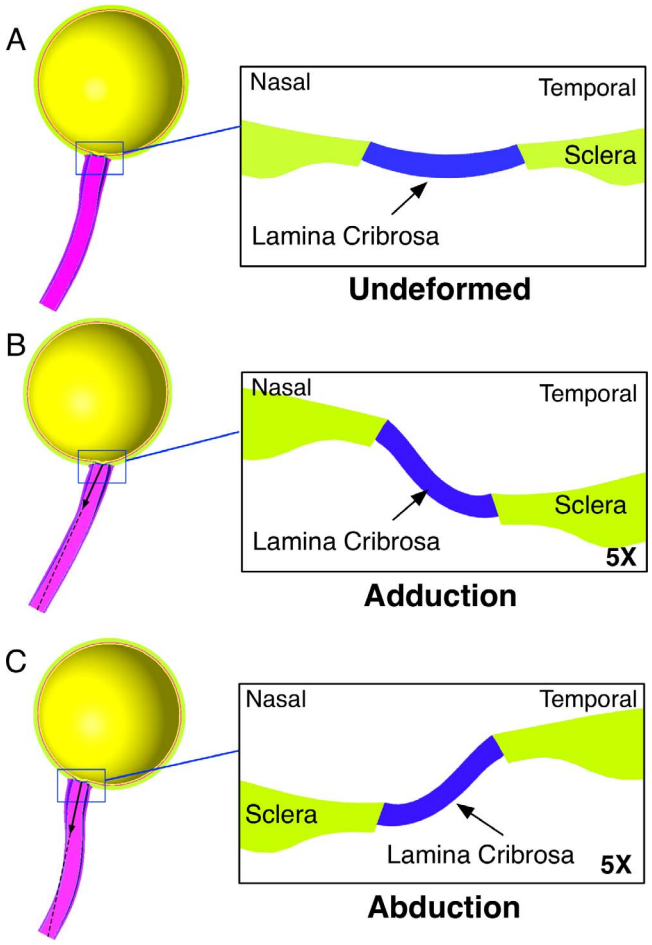

Figure 2. Deformations of the sclera for eye rotations of 13°. (**A**) Underformed model. Note that the deformations in zoomed images in (**B**) and (**C**) were exaggerated five times for illustration purposes. *Black arrows* superimposed on the optic nerve indicate the directions of the reported optic nerve traction forces following eye movements.

Stiffness Factors Influencing ppBM Stresses During Eye Movement

We ranked the influences of the four stiffness factors and their interactions on ppBM stresses following eye movements and the four most significant factors were identified (Fig. 4). In Figure 4, horizontal bars represent the effects of individual stiffness factors or interactions of these factors. A longer bar indicates a more significant effect when varying stiffness from a low to a high value. A green bar is considered beneficial (stress reduction) and a red bar detrimental (stress increase).

We found that soft scleras increased ppBM stresses following eye movements (in both adduction and abduction). This was also true for stiff dura and pia maters. LC stiffness had no significant impact on ppBM stresses during eye movements. Some interaction effects were significant (scleral and dural stiffness interactions in adduction; dural and pial stiffness interactions in abduction); however, their magnitudes remained relatively small.

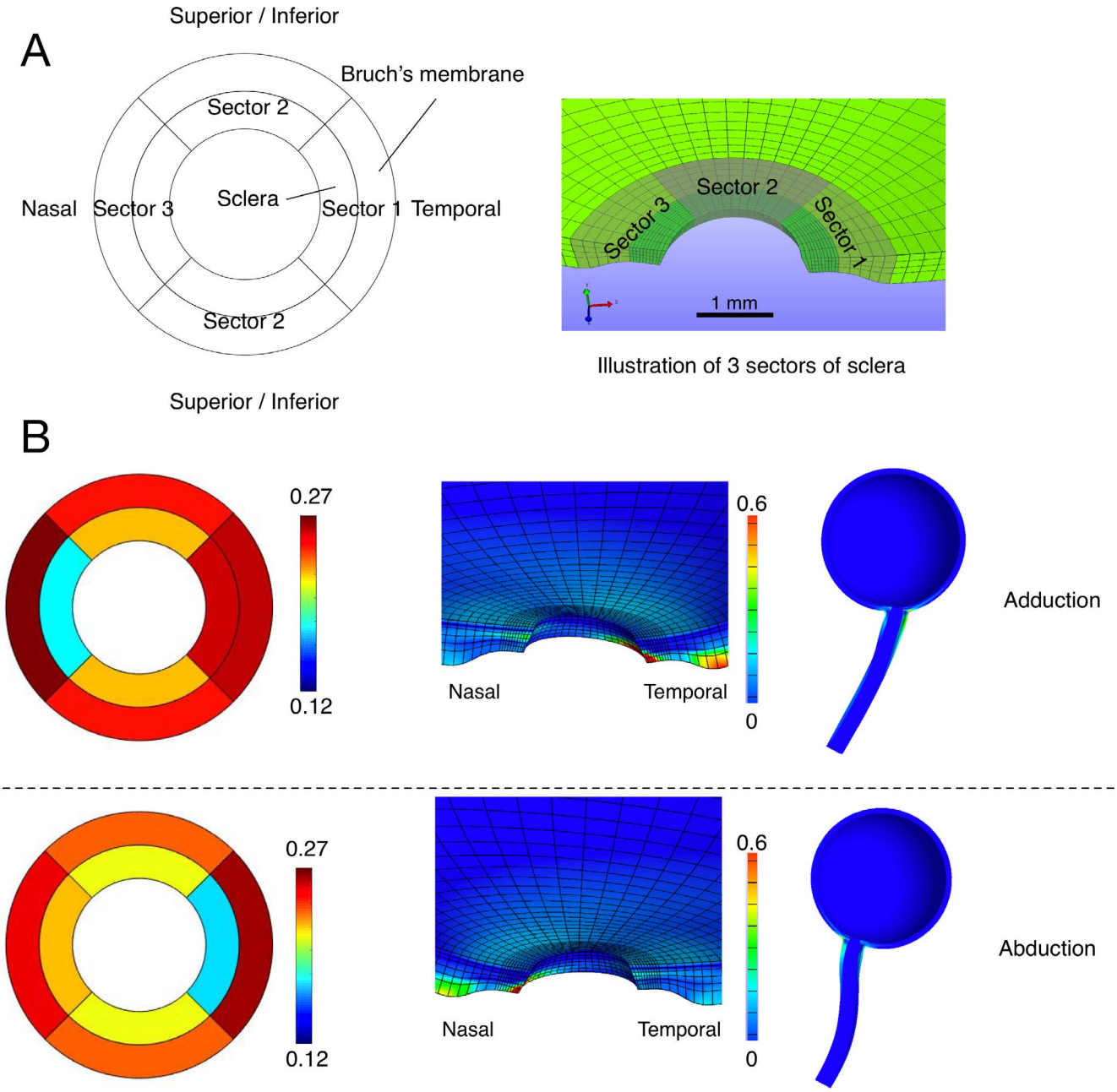

FIGURE 3. (**A**) The ppS and ppBM were divided into three sectors (superior/inferior, nasal, and temporal). (**B**) Average stress values in each sector for two loading scenarios (adduction and abduction of 13 degrees) with corresponding stress color maps. The scleral results were plotted in the inner ring, and those for ppBM were plotted in the outer ring. Unit: MPa.

DISCUSSION

Our study used FE analysis to understand how horizontal eye movements can influence the biomechanical environment of peripapillary tissues. Our models demonstrated that, during eye movements, the ONH was sheared in the transverse plane through the pulling action of the optic nerve and its meninges. The traction forces of the optic nerve sheath were large, which resulted in stresses within the peripapillary tissues localized in the nasal and temporal quadrants. These stresses also were highly influenced by the stiffness of the surrounding connective tissue structures (sclera, dura, pia, but not LC).

Our model predicted a shearing deformation of peripapillary tissues during horizontal eye movements, which was characterized by opposite displacements of nasal and temporal peripapillary tissues (Fig. 2). This deformation pattern is in agreement with that observed in three recent OCT studies.[13–15] Furthermore, LC strains (see Supplementary Material SC) in this study were on the same order of magnitude as those measured in vivo.[14] Additionally, the deformed and undeformed geometries of this model matched well with MRI observations.[16] This suggests that our FE model, although simplified, may be useful to provide a first but preliminary understanding of the stress levels exhibited by peripapillary tissues following eye movements.

For a horizontal eye rotation of 13°, the estimated traction forces generated by the pulling action of the optic nerve sheath were 90 mN in abduction and 150 mN in adduction.

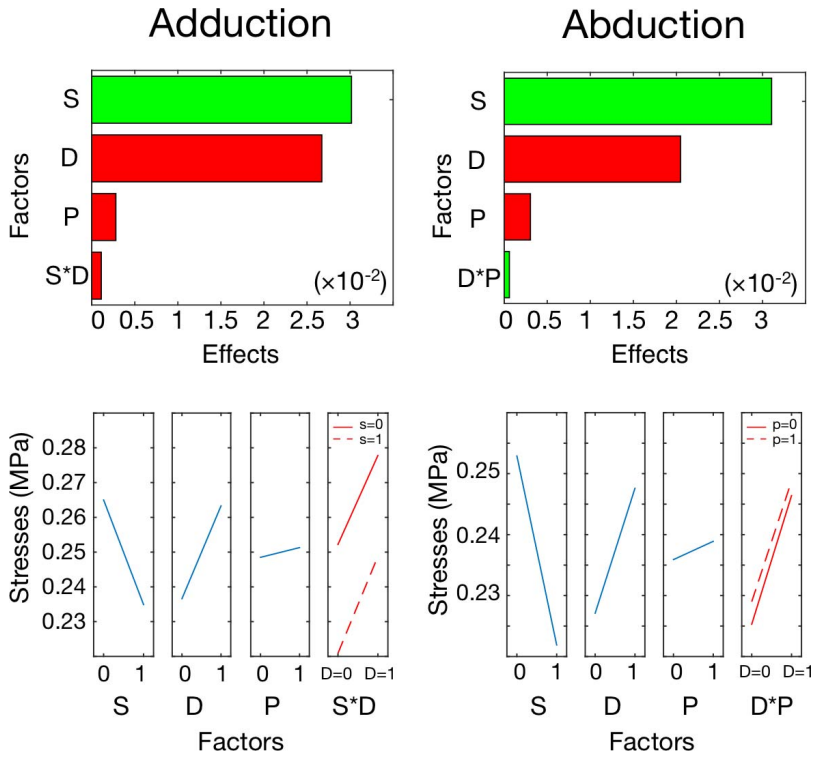

Figure 4. *Upper row*: Ranking of the effects of connective tissue stiffness factors (only the four most significant factors were shown) on the mean effective stress of ppBM. *Green bars* indicate positive effects (stress reduction) and *red bars* indicate negative effects (stress increase). *Lower row*: Effective stress values in ppBM for varied tissue stiffness. Stiffening the sclera considerably reduced ppBM stresses, whereas stiffening the dura had the opposite effect. Interactions between the sclera and dura, or between the dura and pia were relatively small (*red curves* remain close to parallel). 0, low level; 1, high level; S, sclera; D, dura; P, pia; S*D, interaction effects of sclera and dura; D*P, interaction effects of dura and pia. Unit: MPa.

These forces are of the same order of magnitude as those exerted on the globe by the rectus extraocular muscles. Collins et al.[33] demonstrated that, for horizontal eye movements of 50°, the maximum forces that could be developed by the lateral and medial muscles were on average 580 and 730 mN (measured from 29 healthy subjects), respectively. The corresponding muscle forces for eye rotations of 13° would be less than 151 and 190 mN because of the nonlinear relationship between eye rotation amplitude and active force level.[33] Interestingly, the predicted optic nerve sheath traction force in adduction was larger than that in abduction, suggesting that rectus muscles must overcome a larger resistance force in adduction. This is consistent with the fact that the force generated by the medial muscle is typically higher than that of the lateral muscle during horizontal eye movements.[33] Furthermore, the large optic nerve traction force has been demonstrated to be able to retract the eye globe within its orbit in highly myopic eyes with staphyloma.[17] Future studies on eye motility may consider including the non-negligible effects of optic nerve traction.

Previous studies on the structural changes of the ONH region mainly focused on the effects of IOP. Wang et al.[9] observed a folding of the RPE and a sliding of the end of RPE on BM under acute IOP elevation, which was associated with a transient enlargement of the peripapillary beta zone. Moreover, Panda-Jonas et al.[34] observed changes in areas of peripapillary gamma zone in young glaucoma patients after marked surgical reduction of IOP. Our model showed that ONH deformations induced by eye movements are comparable or larger than those induced by a transient IOP[35] or CSFP increases[36] (see Supplementary Material SC), indicating a potential role for ocular movements in the development and progression of peripapillary zones. It could be possible that both the peripapillary beta zone and peripapillary gamma zone are caused partially by abnormal stretching of the ONH region by the optic nerve and its sheaths during eye movements. Note that the links between mechanical stress/strain and peripapillary zones are speculative; further experimental or clinical studies may aid in understanding their potential relationships. In our previous study using in vivo OCT imaging,[14] we observed on average larger gaze-induced ONH deformations in subjects with peripapillary zones. That study was, however, limited to a small sample size (5 eyes without peripapillary zones versus 11 eyes with peripapillary zones), and repeating such work with a larger sample size may provide a better understanding of the correlation between eye movements and peripapillary zones.

Eye movements might partly contribute to axial elongation in myopia. A few studies have reported small axial elongations as a result of either a shift in gaze direction[18,37] or accommodation.[38,39] It has been hypothesized that the change in axial length might be due to mechanical forces generated by the ciliary muscles or extraocular muscles,[40] noting that the extraocular muscle forces are not acting on the axial direction and their effects on globe geometry might be complex and limited. Because our work predicts an optic nerve sheath traction force of the same order of magnitude as extraocular muscle forces, and this traction force directly pulls the globe along its anterior-posterior direction, it would be plausible to suggest that optic nerve traction may have a role to play in axial elongation. If this hypothesis were to be proven correct, optic nerve traction in convergence, such as during prolonged near-reading in myopes, may stretch the globe significantly and

accelerate myopic progression. Moreover, axial elongation itself might be able to cause peripapillary zones through the sliding of BM and stretching of the scleral canal border tissues,[1,41] supporting the hypothesis that peripapillary zones might be correlated with eye movements.

It has been reported that, in incipient myopia, peripapillary zone enlargements were associated with the development of tilted discs, mainly the development and enlargement of peripapillary gamma zone in association with a rotation of the optic disc around its vertical axis.[41] The shearing deformation observed in this study (Fig. 2) and other OCT observations[13–15] might be able to explain the optic disc rotation about the vertical axis (axis along the superior-inferior direction) observed in myopic eyes.[42] It is plausible that continuous stretching of peripapillary tissues following repeated eye movements might contribute to the development of rotated optic discs and peripapillary zones simultaneously through a tissue remodeling process. Note that our model simulated only horizontal eye movements and was symmetric about a transverse plane, which can only yield disc tilting about the vertical axis. The complexity of physiological eye movements (e.g., combination of adduction and depression) in association with variations in eye and orbit anatomy (e.g., axial length or location of the optic nerve origin in the nasal upper region of the orbit) may contribute to the variety of tilting directions seen in patients with tilted optic discs.[43] Additionally, Sibony et al.[44] reported that patients with myopic tilted discs may spontaneously develop peripapillary subretinal hemorrhages. The authors speculated that these were caused by gaze-evoked shearing of blood vessels at the ONH site. Our simulation results support their hypothesis, and future studies are needed to explore the effects of eye movements on the hemodynamics of the ONH region.

Following eye movements, the average ppBM stresses in adduction and abduction did not differ significantly (4.5% difference). However, the difference in ppS stresses was relatively large (ppS stress in adduction was 16% higher than in abduction). This trend was similar to our previous studies,[14,16] in which LC strains in adduction were higher than those in abduction. Other independent studies also concluded that ONH deformation was more affected by adduction.[13,15] Additionally, a higher ppS stress in adduction also was consistent with a larger optic nerve sheath traction force predicted in this study. We speculated that the overall higher stresses in ppS and higher traction forces in adduction were because of a more elongated optic nerve in adduction than in abduction for the same magnitude of eye rotation. A detailed geometric analysis was performed to explain our hypothesis, which can be found in a separate study.[14]

Quadrant-wise stress predictions showed that, in adduction, stress in the temporal ppS was 96% higher than that in the nasal ppS (0.25 vs. 0.13 MPa). In abduction, nasal ppS stress was 64% higher than that in the temporal ppS (0.20 vs. 0.12 MPa). On the contrary, the stress differences in temporal and nasal ppBM were small (5% for adduction and 8% for abduction). Because the traction force exerted by the optic nerve sheaths was not evenly applied on the ppS, it is logical that the ppS stresses would be different in nasal and temporal quadrants. Furthermore, as the ppS is structurally stronger than ppBM (ppS is 100 times thicker than ppBM with an elastic modulus of the same order of magnitude) and the dura sheath directly anchors to the border between the posterior sclera and the peripapillary scleral flange, it is reasonable that traction forces mainly affect the uniformity of stress distribution in the outer part of the ppS and not in the ppBM (Fig. 3). Considering both adduction and abduction models, the average stress experienced by the temporal ppS (which was highest in adduction; 0.25 MPa) was 27% higher than that in the nasal quadrant (which was highest in abduction; 0.20 MPa), whereas the corresponding differences for ppBM were within 5%. The higher stress experienced by the temporal ppS may explain why peripapillary zones are more commonly found on the temporal side,[3] although this would need to be further investigated. It is worth mentioning that adduction-evoked phosphenes[13,45–47] are normally greater on the temporal side of the blind spot, suggesting that nasal peripapillary tissues may be more affected. This is in contradiction with our prediction of higher temporal stresses in adduction. We speculate that it is because retinal cell function is not only affected by the magnitude of stress but also its type (e.g., compression, tension, shearing, or their combinations). Generally, in adduction, the optic nerve sheath pulls the temporal tissues and compresses the nasal tissues, resulting in different stress patterns in nasal and temporal tissues. However, the links between stress/strain patterns to retinal cell functions have not yet been established.

Our sensitivity study showed that a stiffer sclera reduced the overall BM stress following eye movements. This finding is relatively intuitive, as a stiffer sclera will tend to limit the deformations of the whole ONH, thus shielding ppBM from further stress. We also found that the stiffer the dura mater, the higher the ppBM stresses following eye movements. This is not surprising, as a stiffer dura will tend to restrict eye movements by exerting a larger pulling force on the globe.

Our eyes exhibit frequent movements in daily activities (approximately 170,000 saccades per day[48]) and the magnitudes are typically within 15°.[49] Large shifts of gaze are usually accomplished by a combination of head and eye movements. For example, reading text from an A4 size page (width: 170 mm) and from a normal distance will result in an eye rotation angle (eccentricity) of approximately 11° and a head rotation angle of approximately 0.65°.[50] However, reading text from a larger document (width: 535 mm) can result in a head rotation angle of approximately 15.5° and an eye rotation angle that is increased to only approximately 23°.[50] Note that the eye rotation angle used in our simulations was 13°, which is within the normal range of the eye rotation in daily activities. We speculated that if gaze-induced stresses were to exceed a safe threshold over a significant period, tissue growth and remodeling of the peripapillary connective tissues should be expected. However, it should be noted that peripapillary tissue stresses induced by eye movements are transient, as opposed to chronic increases in IOP or CSFP. It is still unclear whether these transient stresses could be harmful to peripapillary tissues.

Limitations

In this study, several limitations warrant further discussion. First, the optic nerve sheath traction force and peripapillary tissue stresses were predicted by FE analysis and were not measured in vivo. Although tissue stress cannot be measured experimentally, the magnitude of the optic nerve traction force could potentially be estimated in vivo. However, this would require a highly invasive and damaging orbital surgery that would be extremely challenging to perform in humans. Our proposed computational approach (partially validated with MRI in our previous work[16]) is currently the safest alternative to test hypotheses related to eye movements and optic nerve traction. Note that our predictions are likely to become more accurate once we consider patient-specific morphologies (through MRI and OCT) and biomechanical properties.[51]

Second, in all FE analyses, the center of eye rotation remained fixed during eye movements. However, it might be

possible that the eye moves actively in the posterior direction, as mediated by the extraocular muscles, to reduce the magnitude of the optic nerve sheath traction force. MRI images of optic nerve straightening during eye movements[17] suggest that even if this active displacement mechanism exists, it will reduce only the magnitude of optic nerve/ONH stretching rather than completely eliminate it. Future FE models could consider incorporating the full geometry of rectus muscles and their active forces to better understand the influence of eye globe rigid motion during eye movements.

Third, the material properties used in this study were derived from experimental studies, except for the LC. However, the value we used for the LC is in agreement with a recent study that measured LC stiffness in vivo.[51] Moreover, the LC was simulated as a homogeneous anisotropic structure, which ignored its porous architecture for simplicity. Also, for some tissues, material properties were extracted from other species other than humans. All these simplifications may influence the absolute value of our stress predictions in this exploratory study. Further studies should incorporate more accurate material properties for these tissues when such data become available.

Fourth, this model may not have considered the right amount of optic nerve "slack" that is present in vivo. Although our models incorporated the "slack" of the optic nerve at both the macroscopic (by taking into account the initial curvature of the optic nerve) and microscopic levels (by taking into account collagen uncrimping with stretch in the stress/strain equations), it is still unclear whether such a "slack" is representative of the in vivo human optic nerve status. Further works are needed to understand if the amount of slack incorporated in our FE models is representative of the in vivo status in the primary gaze position.

Fifth, our model was assumed to be symmetric about a horizontal two-dimensional plane. Therefore, stress differences induced by eye movements between superior and inferior regions could not be simulated. Moreover, the potential stretch effects of the oblique and vertical recti during horizontal eye movements were not accounted for. Future studies should use a more accurate eye geometry to allow investigations of the effects of asymmetries between the superior and inferior peripapillary regions.

Sixth, the CSFP value used in this article represents an averaged pressure in a healthy individual in the supine position. Although many studies used CSFP as a surrogate for the actual pressure in the perioptic subarachnoid space (PSAS), the exact relationship between these two pressures remains unclear. Killer et al.[52,53] demonstrated that the PSAS pressure is inhomogeneous and may be different from the intracranial pressure. In standing or sitting positions, CSFP is zero or negative as reported in the literature.[54,55] However, the exact PSAS pressure is unknown. Sibony[13] showed that elevated CSFP in papilledema increased gaze-evoked ONH deformations, which indicates that CSFP is an important parameter affecting ONH deformations induced by eye movements. The interplay of IOP, CSFP, and eye movements in ONH biomechanics and their potential links to eye diseases need to be investigated in future studies.

Finally, our study did not account for regional variations in scleral thickness and elastic stiffness that are known to exist in humans.[56,57] Such regional variations might contribute to regional differences in peripapillary zones across individuals and is worth further investigation. Similarly, the potential influences of axial length and the variations in the locations of the orbital canal were not investigated in this study and further works are required to understand their roles in eye movements.

Conclusions

Our study used FE to investigate the optic nerve sheath traction forces that act on the eye globe and the stresses in the ppBM and ppS during eye movements. Our models predicted large optic nerve sheath traction forces following eye movements, which resulted in high peripapillary tissue stresses. Further studies are needed to explore a possible link between eye movements and the development of peripapillary zones.

Acknowledgments

Supported by the Singapore Eye Research Institute Pilot Grant (R1228/34/2015), from the Ministry of Education, Academic Research Funds, Tier 1 (R-397-000-181-112) and from a National University of Singapore Young Investigator Award (NUSYIA_FY13_P03, R-397-000-174-133).

Disclosure: **X. Wang**, None; **L.K. Fisher**, None; **D. Milea**, None; **J.B. Jonas**, None; **M.J.A. Girard**, None

References

1. Jonas JB, Wang YX, Zhang Q, et al. Parapapillary gamma zone and axial elongation–associated optic disc rotation: the Beijing Eye Study. *Invest Ophthalmol Vis Sci*. 2016;57:396–402.
2. Jonas JB, Naumann GOH. Parapapillary chorioretinal atrophy in normal and glaucoma eyes. 2. Correlations. *Invest Ophthalmol Vis Sci*. 1989;30:919–926.
3. Jonas JB, Nguyen XN, Gusek GC, Naumann GOH. Parapapillary chorioretinal atrophy in normal and glaucoma eyes. 1. Morphometric data. *Invest Ophthalmol Vis Sci*. 1989;30:908–918.
4. Yamada H, Akagi T, Nakanishi H, et al. Microstructure of peripapillary atrophy and subsequent visual field progression in treated primary open-angle glaucoma. *Ophthalmology*. 2016;123:542–551.
5. Kim YW, Lee EJ, Kim T-W, Kim M, Kim H. Microstructure of β-zone parapapillary atrophy and rate of retinal nerve fiber layer thinning in primary open-angle glaucoma. *Ophthalmology*. 2014;121:1341–1349.
6. Xu L, Li Y, Wang S, Wang Y, Wang Y, Jonas JB. Characteristics of highly myopic eyes: the Beijing Eye Study. *Ophthalmology*. 2007;114:121–126.
7. Jonas JB. Clinical implications of peripapillary atrophy in glaucoma. *Curr Opin Ophthalmol*. 2005;16:84–88.
8. Lee KYC, Tomidokoro A, Sakata R, et al. Cross-sectional anatomic configurations of peripapillary atrophy evaluated with spectral domain-optical coherence tomography. *Invest Ophthalmol Vis Sci*. 2010;51:666–671.
9. Wang YX, Jiang R, Wang NL, Xu L, Jonas JB. Acute peripapillary retinal pigment epithelium changes associated with acute intraocular pressure elevation. *Ophthalmology*. 2015;122:2022–2028.
10. Hayreh SS, Jonas JB, Zimmerman MB. Parapapillary chorioretinal atrophy in chronic high-pressure experimental glaucoma in rhesus monkeys. *Invest Ophthalmol Vis Sci*. 1998;39:2296–2303.
11. Jonas JB, Ohno-Matsui K, Spaide RF, Holbach L, Panda-Jonas S. Macular Bruch's membrane defects and axial length: association with gamma zone and delta zone in peripapillary region. *Invest Ophthalmol Vis Sci*. 2013;54:1295–1302.
12. Jonas JB, Wang YX, Zhang Q, Liu Y, Xu L, Wei WB. Macular Bruch's membrane length and axial length. The Beijing Eye Study. *PLoS One*. 2015;10:e0136833.
13. Sibony PA. Gaze evoked deformations of the peripapillary retina in papilledema and ischemic optic neuropathy. *Invest Ophthalmol Vis Sci*. 2016;57:4979–4987.

14. Wang X, Beotra MR, Tun TA, et al. In vivo 3-dimensional strain mapping confirms large optic nerve head deformations following horizontal eye movements. *Invest Ophthalmol Vis Sci*. 2016;57:5825–5833.
15. Chang MY, Shin A, Park J, et al. Deformation of optic nerve head and peripapillary tissues by horizontal duction. *Am J Ophthalmol*. 2016;174:85–94.
16. Wang X, Rumpel H, Lim WEH, et al. Finite element analysis predicts large optic nerve head strains during horizontal eye movements. *Invest Ophthalmol Vis Sci*. 2016;57:2452–2462.
17. Demer JL. Optic nerve sheath as a novel mechanical load on the globe in ocular duction. *Invest Ophthalmol Vis Sci*. 2016; 57:1826–1838.
18. Ghosh A, Collins MJ, Read SA, Davis BA. Axial length changes with shifts of gaze direction in myopes and emmetropes. *Invest Ophthalmol Vis Sci*. 2012;53:6465–6471.
19. Jiang R, Wang YX, Wei WB, Xu L, Jonas JB. Peripapillary choroidal thickness in adult chinese: The Beijing Eye Study. *Invest Ophthalmol Vis Sci*. 2015;56:4045–4052.
20. Jonas JB, Holbach L, Panda-Jonas S. Bruch′s membrane thickness in high myopia. *Acta Ophthalmol*. 2014;92:e470–e474.
21. Girard MJA, Downs JC, Burgoyne CF, Suh JKF. Peripapillary and posterior scleral mechanics-part I: development of an anisotropic hyperelastic constitutive model. *J Biomech Eng*. 2009;131:051011.
22. Zhang L, Albon J, Jones H, et al. Collagen microstructural factors influencing optic nerve head biomechanics. *Invest Ophthalmol Vis Sci*. 2015;56:2031–2042.
23. Kakizaki H, Takahashi Y, Nakano T, et al. Anatomy of Tenons capsule. *Clin Experiment Ophthalmol*. 2012;40:611–616.
24. Schoemaker I, Hoefnagel PPW, Mastenbroek TJ, et al. Elasticity, viscosity, and deformation of orbital fat. *Invest Ophthalmol Vis Sci*. 2006;47:4819–4826.
25. Hayreh SS. The sheath of the optic-nerve. *Ophthalmologica*. 1984;189:54–63.
26. Hayreh SS. *Structure of the Optic Nerve. Ischemic Optic Neuropathies*. Berlin: Springer-Verlag; 2011:7–34.
27. Hollows FC, Graham PA. Intra-ocular pressure, glaucoma, and glaucoma suspects in a defined population. *Br J Ophthalmol*. 1966;50:570–586.
28. Ren RJ, Jonas JB, Tian GG, et al. Cerebrospinal fluid pressure in glaucoma: A prospective study. *Ophthalmology*. 2010;117: 259–266.
29. Riemann CD, Foster JA, Kosmorsky GS. Direct orbital manometry in patients with thyroid-associated orbitopathy. *Ophthalmology*. 1999;106:1296–1302.
30. Chen K, Rowley AP, Weiland JD, Humayun MS. Elastic properties of human posterior eye. *J Biomed Mater Res A*. 2014;102:2001–2007.
31. Antony J. *Design of Experiments for Engineers and Scientists*. 2nd ed. Waltham, MA: Elsevier; 2014:6–15.
32. Maas SA, Ellis BJ, Ateshian GA, Weiss JA. FEBio: finite elements for biomechanics. *J Biomech Eng*. 2012;134:011005.
33. Collins CC, Carlson MR, Scott AB, Jampolsky A. Extraocular muscle forces in normal human subjects. *Invest Ophthalmol Vis Sci*. 1981;20:652–664.
34. Panda-Jonas S, Xu L, Yang H, Wang YX, Jonas SB, Jonas JB. Optic nerve head morphology in young patients after antiglaucomatous filtering surgery. *Acta Ophthalmol*. 2014; 92:59–64.
35. Girard MJA, Beotra MR, Chin KS, et al. In vivo 3-dimensional strain mapping of the optic nerve head following intraocular pressure lowering by trabeculectomy. *Ophthalmology*. 2016; 123:1190–1200.
36. Feola AJ, Myers JG, Raykin J, et al. Finite element modeling of factors influencing optic nerve head deformation due to intracranial pressure. *Invest Ophthalmol Vis Sci*. 2016;57: 1901–1911.
37. Ghosh A, Collins MJ, Read SA, Davis BA, Chatterjee P. Axial elongation associated with biomechanical factors during near work. *Optom Vis Sci*. 2014;91:322–329.
38. Mallen EAH, Kashyap P, Hampson KM. Transient axial length change during the accommodation response in young adults. *Invest Ophthalmol Vis Sci*. 2006;47:1251–1254.
39. Drexler W, Findl O, Schmetterer L, Hitzenberger CK, Fercher AF. Eye elongation during accommodation in humans: differences between emmetropes and myopes. *Invest Ophthalmol Vis Sci*. 1998;39:2140–2147.
40. Greene PR. Mechanical considerations in myopia - relative effects of accommodation, convergence, intraocular-pressure, and the extra-ocular muscles. *Am J Optom Physiol Opt*. 1980; 57:902–914.
41. Kim TW, Kim M, Weinreb RN, Woo SJ, Park KH, Hwang JM. Optic disc change with incipient myopia of childhood. *Ophthalmology*. 2012;119:21–26.e3.
42. Dai Y, Jonas JB, Ling Z, Sun X. Ophthalmoscopic-perspectively distorted optic disc diameters and real disc diameters. *Invest Ophthalmol Vis Sci*. 2015;56:7076–7083.
43. Han JC, Lee EJ, Kim SH, Kee C. Visual field progression pattern associated with optic disc tilt morphology in myopic open-angle glaucoma. *Am J Ophthalmol*. 2016;169:33–45.
44. Sibony P, Fourman S, Honkanen R, El Baba F. Asymptomatic peripapillary subretinal hemorrhage: a study of 10 cases. *J Neuroophthalmol*. 2008;28:114–119.
45. von Helmholtz H. *Helmholtz's Treatise on Physiological Optics. Translated from the Third German Edition.* Southall JPC, ed. New York: The Optical Society of America; 1924.
46. Tyler CW. Some new entoptic phenomena. *Vis Res*. 1978;18: 1633–1639.
47. Shin YU, Lim HW, Kim JH. Changes of optic nerve head induced by eye movement. *Neurology*. 2016;87:2490–2491.
48. Schiller PH, Tehovnik EJ. Neural mechanisms underlying target selection with saccadic eye movements. *Prog Brain Res*. 2005;149:157–171.
49. Bahill AT, Stark L. The trajectories of saccadic eye movements. *Sci Am*. 1979;240:108–117.
50. Proudlock FA, Shekhar H, Gottlob I. Coordination of eye and head movements during reading. *Invest Ophthalmol Vis Sci*. 2003;44:2991–2998.
51. Zhang L, Thakku SG, Beotra MR, et al. Verification of a virtual fields method to extract the mechanical properties of human optic nerve head tissues in vivo. *Biomech Model Mechanobiol*. In press.
52. Killer HE, Jaggi GP, Flammer J, Miller NR, Huber AR. The optic nerve: a new window into cerebrospinal fluid composition? *Brain*. 2006;129:1027–1030.
53. Killer HE, Jaggi GP, Flammer J, Miller NR, Huber AR, Mironov A. Cerebrospinal fluid dynamics between the intracranial and the subarachnoid space of the optic nerve. Is it always bidirectional? *Brain*. 2007;130:514–520.
54. Andresen M, Hadi A, Petersen LG, Juhler M. Effect of postural changes on ICP in healthy and ill subjects. *Acta Neurochir (Wien)*. 2014;157:109–113.
55. Chapman PH, Cosman ER, Arnold MA. The relationship between ventricular fluid pressure and body position in normal subjects and subjects with shunts: a telemetric study. *Neurosurgery*. 1990;26:181–189.
56. Girard MJA, Suh JKF, Bottlang M, Burgoyne CF, Downs JC. Scleral biomechanics in the aging monkey eye. *Invest Ophthalmol Vis Sci*. 2009;50:5226–5237.

Investigative Ophthalmology & Visual Science

57. Norman RE, Flanagan JG, Rausch SM, et al. Dimensions of the human sclera: thickness measurement and regional changes with axial length. *Exp Eye Res*. 2010;90:277–284.
58. Chan WH, Hussain AA, Marshall J. Youngs modulus of Bruchs membrane: implications for AMD. *Invest Ophthalmol Vis Sci*. 2007;48:2187–2187.
59. Friberg TR, Lace JW. A comparison of the elastic properties of human choroid and sclera. *Exp Eye Res*. 1988;47:429–436.
60. Miller K. Constitutive model of brain tissue suitable for finite element analysis of surgical procedures. *J Biomech*. 1999;32:531–537.

Investigative Ophthalmology & Visual Science